Versatile IR spectroscopy combined with synchrotron XAS-XRD: Chemical, electronic and structural insights during thermal treatment of MOF materials

Satoshi Hinokuma,[a,b] Geir Wiker,[c] Takuya Suganuma,[d] Atul Bansode,[e] Dragos Stoian,[c] Silvia Caminero Huertas,[e] Sonia Molina,[e] Alexandr Shafir,[e] Magnus Rønning,[f] Wouter van Beek,[c] and Atsushi Urakawa*[e,g]

[a] Department of Applied Chemistry and Biochemistry, Graduate School of Science and Technology, Kumamoto University, 2-39-1 Kurokami, Chuo-ku, Kumamoto 860-8555, Japan
[b] International Research Organization for Advanced Science and Technology, Kumamoto University, Japan
[c] The Swiss-Norwegian Beamlines (SNBL) at ESRF, BP 220, F-38043 Grenoble, France
[d] Toyota Motor Corporation, 1200, Mishuku, Susono, Shizuoka, Japan
[e] Institute of Chemical Research of Catalonia (ICIQ), The Barcelona Institute of Science and Technology, Av. Països Catalans 16, 43007 Tarragona, Spain
*Emai: aurakawa@iciq.es
[f] Department of Chemical Engineering, Norwegian University of Science and Technology, 7491 Trondheim, Norway
[g] JST, PRESTO, 4-1-8 Honcho Kawaguchi, Saitama 332-0012, Japan

Abstract:

Understanding the physicochemical origin of functional materials generally requires multi-faceted information on their material characteristics investigated by various analytical methods. In this respect, simultaneous multi-probe approach to study materials by complementary methods is of great value, particularly to follow dynamically varying processes such as chemical and structural transformation under reactive environment. Herein, we report facile and versatile approaches to combine synchrotron X-ray absorption spectroscopy and diffraction with IR spectroscopy in transmission and diffuse-reflection sampling configurations to study pellet samples under controlled environment. The high practicality of the approach was enabled by the use of a modular IR spectrometer. Rich information on chemical, electronic and structural changes of Zr-BTC and Cu-BTC MOFs during a thermal treatment was gained by the multi-probe approach. The advantages and practical challenges of the combined approaches are discussed.

Introduction

Functionality of inorganic materials is widely investigated and understood by spectroscopic and diffraction methods through rich information on their physicochemical properties including chemical interactions, long-range order and electronic/magnetic structures. Remarkable progresses have been made in modern detection techniques; however, convincing solutions to the puzzles in chemistry and material sciences often require multi-faceted information. In theory, holistic information to solve the puzzles can be obtained separately by various detection methods on a sample under an identical environment, but it is always of great challenge to ensure the comparability of the results. This is especially true when materials are studied under a specific set of conditions where chemical and structural transformation takes place, such as a reaction environment common in catalytic reactions. Obviously, measurements performed simultaneously by different techniques (i.e. multi-probe) are the most ideal solution to make sure that the inorganic material state is absolutely identical. Hence, numerous researchers have reported such approaches, each providing distinct advantages depending on the analytical techniques chosen and the cell design [1].

The use of synchrotron X-ray has shown its unique advantages in performing *in situ* and *operando* spectroscopic and diffraction studies and its use became a standard in the modern chemical and material science [2]. This is facilitated by better accessibility to synchrotron radiation facilities seen over the past few decades. For instance, it is increasingly possible to combine X-ray absorption spectroscopy (XAS) and X-ray diffraction (XRD) with Raman spectroscopy simultaneously or quasi-simultaneously [3]. On the other hand, simultaneous measurements of X-ray spectroscopy with infrared (IR) spectroscopy has been limited, although IR spectroscopy is the most versatile analytical method used under *in situ* conditions to study chemical structures and interactions of gas, liquid, solid and their interfaces [4]. This scarcity mainly originates from the restrictive requirement of optical components as well as from the geometrical inconvenience of the combined measurements, e.g. the placement of an IR spectrometer that would enable simultaneous IR and X-ray spectroscopies. In this respect, Raman spectroscopy has evident advantages because Raman excitation laser and signals can be conveniently transmitted through optical fiber and hence only requires placing a portable probe near the sample. Despite the difficulties to perform simultaneous IR and X-ray spectroscopies, Newton *et al.* pioneered such combination with diffuse reflectance Fourier transform IR spectroscopy (DRIFTS) to study powder samples and extensively applied the combined approaches in *operando* studies of catalytic materials [5].

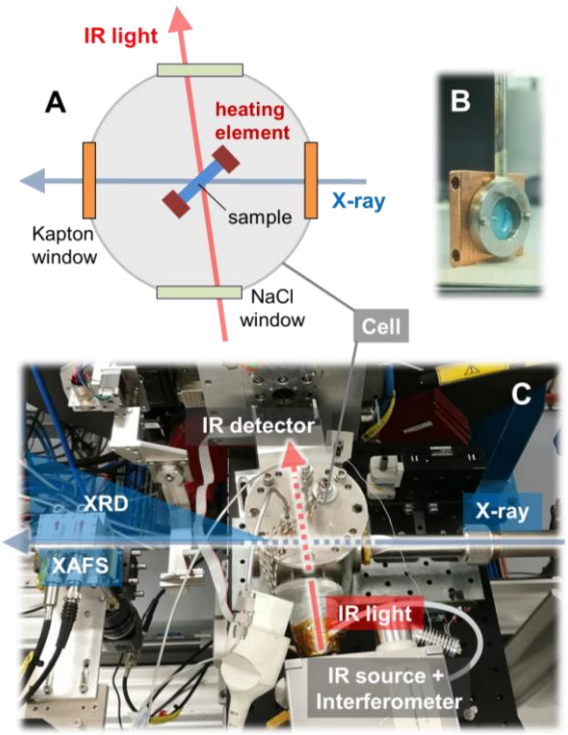

Herein, we report proof-of-principle experiments of the combined XAS-XRD with, for the first time to the best of our knowledge, transmission IR spectroscopy as well as DRIFTS using a pellet-shaped material using a cell suited for combined XAS-XRD [6] adapted to allow IR detection. Particularly, we show the use of a modular IR spectrometer, enabling these combinations in a facile and versatile fashion, manifesting ample opportunities for far-ranging combination of IR spectroscopy with other detection methods. To verify the power of the combined approach and good signal quality, chemical, geometrical and electronic structural changes of benzene-1,3,5-tricarboxylate (BTC)-based Zr and Cu metal-organic framework (MOF) materials were studied during the thermal treatment process.

Figure 1. (A) Schematic drawing of the cell (top view) and IR light and X-ray optical paths to perform the simultaneous IR-XAS-XRD measurements. (B) Pellet sample holder. The holes are to insert heating cartridges. (C) The IR-XAS-XRD system in action where the cell was purged with He at 100 mL min^{-1} during the thermal treatment.

Results and Discussion

IR spectroscopy combined with XAS/XRD on a same sample has been scarcely reported due to geometrical constraints as well as the compatibility of optical materials and sample concentration or thickness, in particular to perform IR spectroscopy with XAS (XRD has less restrictions in practice).

Herein we evaluated two different IR sampling configurations, namely transmission IR spectroscopy and DRIFTS in combination with XAS-XRD, to study pellet samples under controlled environment (sample temperature and atmosphere). The possibility of two IR sampling configurations broadens the scope of materials which can be studied by the combined method. Below, the sections are separated by the measurements using the respective IR sampling configuration.

Transmission IR spectroscopy combined with XAS-XRD

Simultaneous measurements of transmission IR and XAS-XRD were made possible by fixing a heatable sample holder (Figure 1B) in the cell at about 45° to the X-ray and with respect to the surface of the pellet (Figure 1A). Nearly orthogonal to the X-ray, IR light was passed through the sample. In practice the angle was slightly tilted to increase the sampling area by the IR light by quickly and conveniently adjusting the position of the IR spectrometer and detector (Figure 1C). Such an orthogonal configuration of the light paths and alignment capability are very difficult, if at all possible, with conventional box-shaped spectrometers. The freely-movable interferometer with the IR source and the mid-IR (thermoelectrically cooled MCT) detector of the mobile IR spectrometer system (Arcoptix S. A., OEM model) allowed flexible positioning and sensitive signal detection.

The study of pellet sample is by itself challenging in terms of achieving the best quality signals in the multi-probe measurement due to the necessity to optimize the sample amount/thickness. The situation is further complicated when an ultra-thin self-supporting wafer is required in IR spectroscopy. Here we evaluated an option of using a pellet made by a two-step process, by first preparing a 13 mm diameter pellet of NaCl (50 mg) at high pressure and then placing softly a small amount of the sample (3 mg of Zr-BTC, *vide infra*) at low pressure. This method allows for optimisation of the material amount for use in transmission IR and XAS. The requisite for the base supporting pellet is that it should be transparent to both IR and X-ray at the energy of the measurement. Hence, the typical material for IR pellet, KBr, cannot be used conveniently in this case, since Br is a comparably heavy chemical element, thus absorbing most incident X-ray. At the K-edge of Zr (ca. 18 keV), NaCl is highly transparent and can be conveniently used and thus this material was chosen.

Figure 2. (A) Geometrical structure of BTC. (B) Zirconium oxide secondary building unit (SBU) where six octahedrally disposed zirconium atoms are held together. Hydrogen atoms are not shown for the sake of clarity. The figure shows how six BTCs and formates coordinate to Zr (the structure

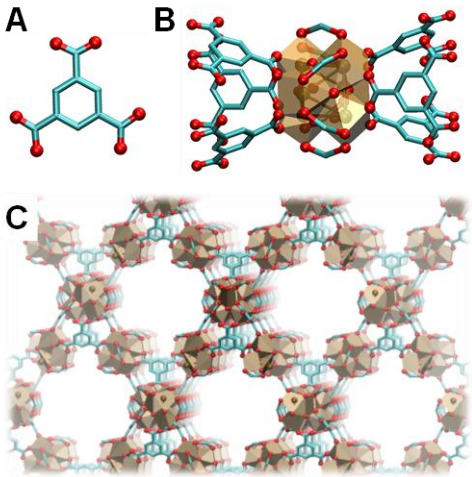

as reported by Yaghi and coworkers as MOF-808 [7]. Note that the Zr-BTC of this study contains acetates instead of formates. (C) The MOF-808 formed made by the SBU and BTC.

Figure 2 shows the constituting molecular units and the structure of the Zr-MOF material studied by the multi-probe approach. The linker of the MOF material is benzene-1,3,5-tricarboxylate (BTC, Figure 2A), connecting the zirconium oxide secondary building unit (SBU) where six octahedrally disposed zirconium atoms are held together by bridging carboxylates. The structure is known as MOF-808 [7] and is related to the more popular Zr-based MOF structures, such as the classical terephthalate-based UiO-66. For MOF-808, six BTC linkers are connected to each SBU (Figure 2B), with acetates providing the rest of the stabilization for the Zr_6 SBU (formates were used in the original work in [7]), resulting in the structure shown in Figure 2C. Hereafter we call the material, simply Zr-BTC. Prior to the thermal treatment, the sample was pretreated by the procedure, so-called, activation. It consists of evacuation for 5 h at room temperature and then for 15 h at 100 °C following a ramp of 1 °C min^{-1}. The sample was then exposed to air; thus the initial state of the sample mainly contains a large amount of H_2O in the porous structure (ca. 10 wt% according to TGA analysis). This type of MOF materials are known to show unique characteristics for water adsorption and absorption [7].

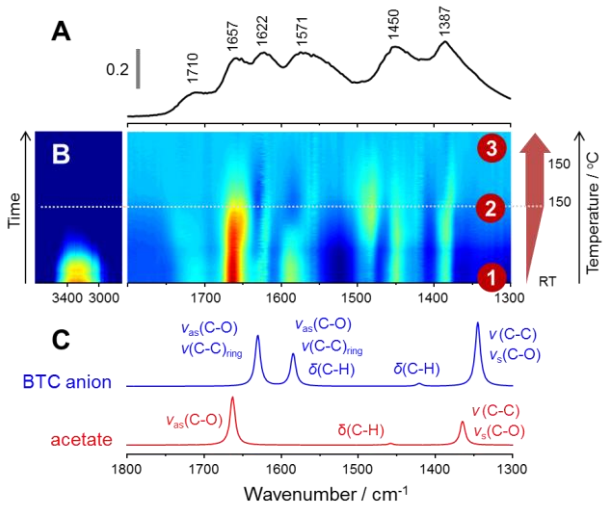

Figure 3. (A) *Ex situ* transmission IR spectrum of Zr-BTC in air after the activation treatment. The bar of 0.2 refers to Absorbance units. (B) *In situ* transmission IR spectrum during the thermal treatment where Zr-BTC was heated from RT to 150 °C at 0.5 °C/min and then kept for 4 h. The background was taken using the last spectrum of this experiment (i.e. at the end of the thermal treatment). (C) Calculated IR spectra of BTC and acetate anions at B3PW91/6-311++G(2d,2p) and the band assignments from the normal mode analysis.

The sample was heated from room temperature (RT) to 150 °C at 0.5 °C min^{-1} under He flow and then kept at the temperature. Chemical, geometrical and electronic information of Zr-BTC was gained by the combined IR-XAS-XRD. Figure 3 summarizes the IR view on the material during the thermal treatment. Figure 3A shows the *ex situ* IR spectrum of the Zr-BTC before the thermal treatment, showing six relatively-broad bands in the characteristic frequency region. It is interesting to note that all six bands underwent intensity change and/or band shift during the thermal treatment (Figure 3B) as the temperature increased. During the treatment, mainly water desorption took place as evident form the drastic decrease of the broad band at ca. 3300 cm^{-1} characteristic of hydrogen-bonded, adsorbed H_2O. Among the six bands, the band at 1657 cm^{-1} disappeared during the thermal treatment, while the changes of the other bands as shift or decrease was less pronounced. According to the DFT calculation (Figure 3C) this band can be assigned to the asymmetric C-O stretching vibration of acetate ligand on the Zr SBU. This indicates that the stability of the acetate ligand is higher than adsorbed water, but they can be gradually removed at 150 °C. Another prominent band of the acetate is the

combined C-C stretching and symmetric C-O stretching mode experimentally observed at ca. 1387 cm^{-1}. Both bands underwent changes slightly with broadening or shift when water was removed from the structure and then remarkably at ca. 150 °C (point 2, in Figure 3B), resulting in the band disappearance. The small band of C-H bending vibration of acetate, theoretically predicted to be at ca. 1460 cm^{-1}, seems emerging at ca. 1480 cm^{-1} when H_2O was removed from the MOF structure and then the band disappears as the prominent acetate band at 1657 cm^{-1} disappears. This implies that the polarity environment changes near the methyl group of acetate during the water removal. On the other hand, the bands due to BTC at 1450, 1571 and 1622 cm^{-1} underwent minor changes in absorbance (apparently the changes seems considerable but this is due to the nature of difference spectrum). Generally all bands showed red-shifts upon H_2O removal, due to the higher interactions between BTC and Zr-SBU upon thermal treatment.

Figure 4. XAS and XRD results during the thermal treatment. (A) Zr K-edge normalized XANES spectra, (B) Fourier transforms (FT) of k^3-weighted EXAFS of Zr-BTC, and (C) XRD patterns of the Zr-BTC/NaCl pellet measured at three time points (1: blue, 2: red, 3: green) during the thermal process as indicated in Figure 3B.

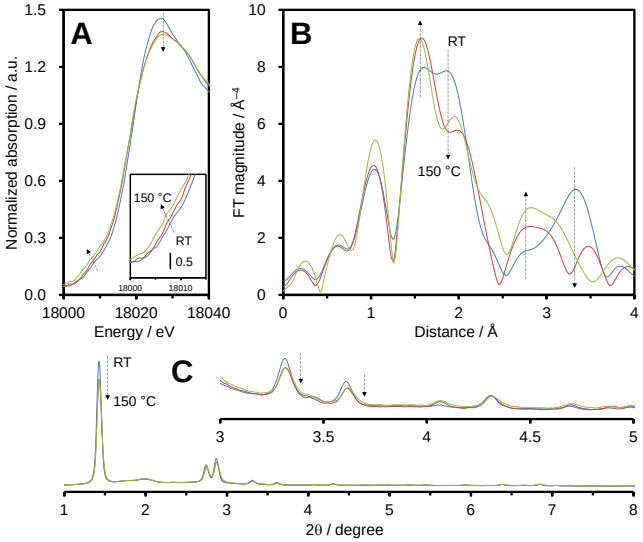

Figure 4 summarises the electronic and structural views by XAS and XRD on Zr-BTC under the thermal treatment. The Zr K-edge X-ray absorption near-edge spectra (XANES, Figure 4A) show the absorption energy and the intensity become lower upon the treatment, implying the formation of a metal center with a reduced coordination number, although the extent of the shift is not drastic. On the other hand, the structural information gained by extended X-ray absorption fine structure (EXAFS) shows a great change in the local environment near Zr (Figure 4B). FT magnitudes of the two prominent peaks at 1.8 and 3.3 Å decreased, accompanying an increase of the peaks at 1.6 and 2.8 Å. A detailed analysis shows that the two peaks are assigned to Zr-O and Zr-Zr distances, respectively. Similar XANES and/or FT-EXAFS profiles of a related Zr-MOF material have been disclosed [8]. Lillerud *et al.* studied by XANES and EXAFS the effect of progressive dehydration of a Zr-MOF during a heating treatment from RT to 300 °C, and similar behavior and coordination change related to Zr were clarified. In fact, in a seminal 2010 report, Lillerud, Lamberti and co-workers were able to establish for the prototypical UiO-66 MOF a change in the nature of the Zr_6 SBU unit in going from the "as-synthesized" materials to the dehydrated form [8b]. Specifically, a combination of XRD, XAS and IR measurements showed a reduction in the immediate Zr coordination sphere from 8 (refined for EXAFS with two independent Zr-O distances) to a smaller value due to the loss of two molecules of water, presumably from the initially present μ^3-OH ligands.

The change meant that the cluster symmetry was reduced from tetrahedral (T_d) to D_{3d}. Recently; a related solution-state study was also reported for the discreet Zr_6 SBU prepared as its acetate form [8g]. It should be mentioned, however, that despite their similarities, there exists an important structural difference between the Zr_6 units present in the UiO family of MOFs and in the Zr MOFs based on 3-fold symmetric linkers, such as BTC used in this study. Indeed, the metallic node in the Zr-BTC system is expected to only contain 6 edges bridged by the linker-bound carboxylates, with the remaining 6 edges occupied by mono-carboxylates. This may lead to a thermal behaviour different from that observed for the more highly connected UiO-66. Even so, the observed spectral changes of Zr-BTC by XAS are reasonable and the removal of acetate ligand was firmly proven in this work by the complementary information of IR.

From XRD (Figure 4C), there are slight peak shifts observed and some reflection intensities are altered mainly due to the electron density changes in the pore, although generally the change was rather minor (ca. 0.2% unit cell volume reduction according to the Rietveld refinement). All these results indicate that the framework (MOF) structure was retained after the thermal treatment, but the structure and chemical environment of the Zr_6 SBU did undergo a change. According to the IR results (Figure 3), the acetate ligands were removed, following the water removal from the pore, and this should have a direct impact on the structure of the SBU. XAS results (Figures 4A and 4B) indicate that upon the acetate removal the Zr in the cluster unit is more electronically saturated most likely due to the loss of coordinating oxygen of acetate, and this induces the readjustment of the coordination environment of Zr by shortening the atomic distance among Zr atoms. These changes are reminiscent to those due to the loss water from the Zr_6 structural building units of UiO-66, although now the acetate ligands may also be engaged in this thermal loss of bridging ligand loss [8b]. Such detailed insights are uniquely gained by the multi-probe approach, especially by the addition of the IR spectroscopy which can provide chemically highly relevant information. The results indicate that upon sufficiently long thermal treatment at 150 °C in inert atmosphere, an electronically richer (less coordinatively saturated) Zr center is formed, thus possibly offering sites for catalytic reaction.

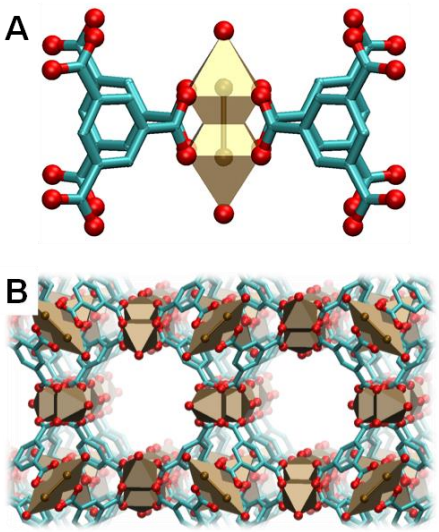

Figure 5. (A) The SBU of Cu-BTC where two copper atoms are held together. The figure shows how four BTCs coordinate to Cu and two water molecules are disposed (only oxygen atoms are shown) [9]. (B) Cu-BTC structure (known as HKUST-1) formed by the SBU and BTC. Hydrogen atoms are not shown for the sake of clarity

DRIFTS combined with XAS-XRD

While transmission IR spectroscopy is ideal from quantitative and less-temperature-dependency points of views, in some cases measurement of pellet sample in combination with XAS-XRD is not possible. For example, when a Cu-MOF is studied, it is not possible to use the same approach as shown above with a NaCl supporting pellet due to the low Cu K-edge absorption energy (ca. 9 keV). For this reason, we evaluated another IR sampling configuration, DRIFTS, so that sample concentration for IR is not limited any longer and one can increase it to an optimum level for XAS-XRD. Here we performed a similar study by a combined DRIFTS-XAS-XRD using a self-supporting wafer of Cu-BTC MOF (known as HKUST-1, Figure 5).

Figure 6 shows the schematic configuration of the cell affording DRIFTS. To enable both IR and X-ray spectroscopies from the same window, a hole was made on a NaCl window which was then sealed with a Kapton material. Using such a window and placing the sample holder close to the window, there was enough space for IR light to travel through the NaCl part of the window and also for X-ray to travel through the hole, reaching the sample and up to respective detector. Such configuration was again possible due to the modular nature of the IR spectrometer used in this study.

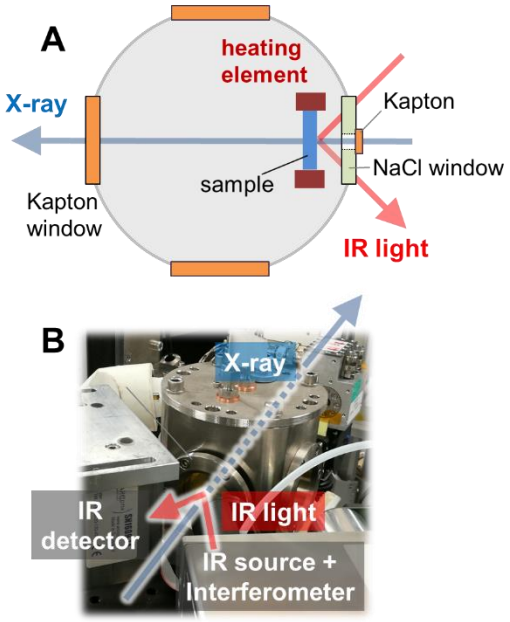

Figure 6. (A) Schematic drawing of the cell (top view) and IR light and X-ray optical paths to perform the simultaneous DRIFTS-XAS-XRD measurements. (B) The DRIFTS-XAS-XRD system in action.

It should be mentioned that the in this work a common pelleting method was used, resulting the Cu-BTC pellet with a smooth surface. This is not ideal for DRIFTS where scattered diffuse-reflection by a rough surface should be maximized. As a consequence, the IR signal originating from the sample was very low. Nevertheless, the signature of adsorbed water in the material could be detected and the evolution during the thermal treatment is summarized in Figure 7. Evidently, water gradually desorbed from Cu-BTC upon heating, first with a decrease of water from the pore as recognized by the disappearance of the broad band at 3300-3600 cm^{-1}, followed by the desorption of strongly-bound water at higher temperature as indicated by the isolated O-H vibrations at ca. 3650 cm^{-1}.

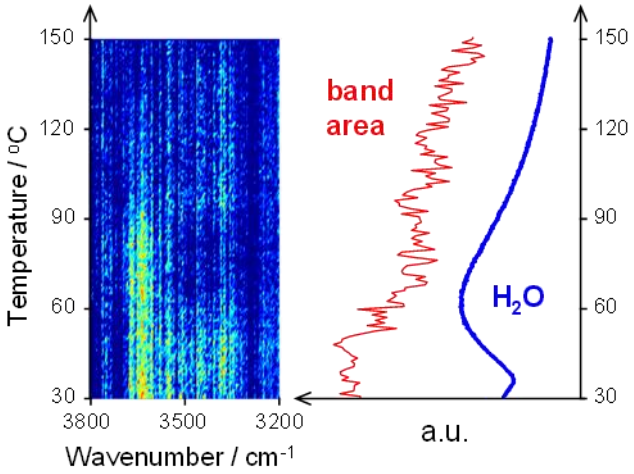

Figure 7. (left) DRIFT spectra of Cu-BTC in the OH stretching region during the thermal treatment (ramp at 1 °C min^{-1}) and (right) the area of the broad band shown on the left and the signal of water (m/e=18) recorded by mass spectrometry during the treatment.

Figure 8A presents Cu K-edge normalized XANES spectra of Cu-BTC during the thermal treatment. The spectra showed a minor pre-edge peak assigned to a charge-transfer excitation [10] and the absorption decreased with a slight shift to lower energies upon increasing temperature. According to a previous report [11], these observations imply that the Cu in Cu-BTC becomes electronically more saturated during the treatment by the removal of the water in the SBU. This behavior is apparently less pronounced compared to the case of Zr-BTC (Figure 4A).

On the other hand, the FT of k^3-weighted EXAFS of Cu-BTC basically did not undergo major changes, although a small decrease of the peak at 1.6 Å attributed to Cu-O distance was observed. Also, from XRD (Figure 8C) there are slight peak shifts observed and reflection intensities are altered, but generally the Cu-BTC structure was retained and the volume change was also minor (ca. 0.3% decrease). Considering all results, it can be concluded that water at the SBU can be removed by the thermal treatment at 150 °C and this causes partial reduction of Cu; however, its extent and effects on the SBU structure are minor compared to the case of Zr-BTC where the removal of the ligand induces more drastic changes in the electronic density of the metal center, large changes in the coordination environment near Zr atoms and consequently the transformation of the SBU structure.

Figure 8. XAS and XRD results during the thermal treatment. (A) Cu K-edge normalized XANES spectra, (B) Fourier transforms (FT) of k^3-weighted EXAFS of Cu-BTC, and (C) XRD patterns of the Cu-BTC pellet measured during the thermal process as indicated in Figure 7.

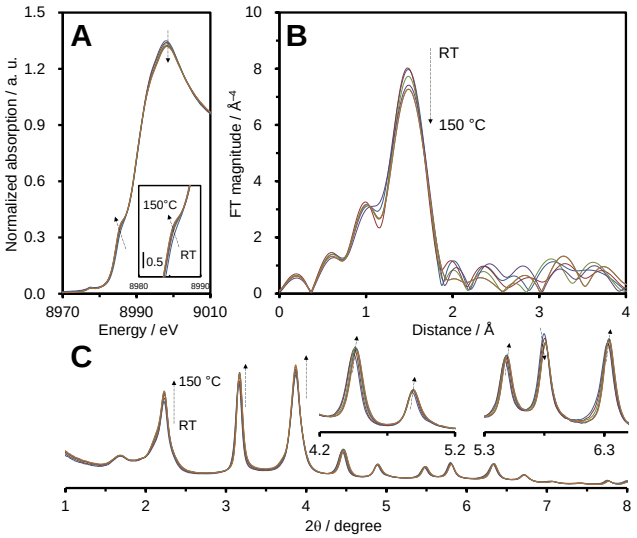

Conclusions

Simultaneous multi-probe measurements by combining synchrotron XAS and XRD with IR spectroscopy in transmission and

diffuse-reflection sampling configuration, facilitated by the modular IR spectrometer system, were successfully performed to study physicochemical processes of the MOF materials under thermal treatment. The two examples presented in this work demonstrate a wide range of possibilities to combine IR spectroscopy based on the modular spectrometer with X-ray spectroscopy and other methods thanks to the high positioning flexibility and miniature character of the IR spectrometer, which are of particular importance at synchrotron radiation facilities. Studying materials in a pellet form is often advantageous in terms of signal quality at the expense of difficulty in sample preparation and handling. This work presented a versatile approach to support a small amount of sample on supporting pellet which is largely transparent to both IR light and X-ray. With such an approach, one can achieve high quality signals by IR-XAS-XRD in transmission configuration. When thicker samples are required for signal quality and optical component reasons, one can perform measurements in the diffuse-reflection sampling configuration for IR spectroscopy. The signal quality was deteriorated due to the smooth surface of the pellet used and further optimisation of sample form (e.g. surface roughing by drop casting) is required but the proof-of-principle of the multi-probe approach was firmly shown. For this work the same cell was used for both the transmission IR and DRIFTS measurements. The experimental geometry can be further optimised by allowing larger incident angles for even more techniques. The generally used activation protocol of MOFs by the thermal treatment was shown to induce even chemical transformation near Zr atoms by the release of ligands accompanying a partial electronic structure change of Zr. Such insights are of particular importance in understanding the functionality of materials and envisioning their potential applications.

Experimental Section

Materials

Zr-BTC ($Zr_6O_4(OH)_4X_6(BTC)_2$, X: acetate, BTC: benzene-1,3,5-tricarboxylate) was synthesised according to the previous report [12]. $ZrOCl_2 \cdot 8H_2O$ was dissolved in a mixture of acetic acid and water in a round bottom flask and to the resultant solution was added benzene-1,3,5-tricarboxylic acid; mixture was then allowed to stir for a few minutes. The flask was equipped with a reflux condenser and the reaction was kept stirring at 130 ^{O}C for 24 hours. The resulting precipitate was separated by centrifugation and washed with water, DMF and acetone. To remove the solvents from the pores (i.e., activation), the material was evacuated for 5 h at room temperature and then for 15 h at 100 °C after a ramp of 1 °C min^{-1}. Cu-BTC ($C_{18}H_6Cu_3O_{12}$, Basolite® C300, Sigma-Aldrich) was purchased and used as received.

Methods

IR-XAS-XRD multi-probe experiments were performed at the Swiss- Norwegian Beamlines (SNBL, BM31) of the European Synchrotron Radiation Facility (ESRF), France. For XAS-XRD combined with transmission IR, Zr-BTC (3 mg) supported on a NaCl pellet (50 mg, >99%, Sigma) was shaped into a disk of 13 mm diameter with ca. 0.2 mm thickness and it was put into the sample holder (Figure 1B). For XAS-XRD combined with DRIFTS, Cu-BTC (16 mg) was also pelletized into the self-supporting disk of 13 mm diameter with ca. 0.1 mm thickness prior to mounting on the sample holder.

XAS spectra were recorded in transmission mode at the Zr and Cu K-edge using a double crystal Si(111) monochromator. Zr and Cu foils were used for energy calibration. One XAFS spectrum was

acquired in 5 min. The XAFS data were processed using the IFEFFIT software package (Athena and Artemis). EXAFS oscillations were extracted by fitting a cubic spline function through the post-edge region. The k^3-weighted EXAFS oscillation in the 3.0-12.0 $Å^{-1}$ region was Fourier transformed. XRD patterns were recorded on a large MAR345 image plate detector with the incident X-ray at the wavelength of 0.51105089 Å. The detector calibration was performed with the LaB_6 standard. One XRD pattern was acquired for 10 min. Transmission IR and/or DRIFTS measurements were performed using the modular FT-IR spectrometer (Arcoptix, OEM model) and each spectrum was recorded for 60 s. The effluent gas concentrations were recorded by a mass spectrometer (OmniStar, Pfeiffer Vacuum).

The theoretical IR spectra of BTC and acetate was calculated with the B3PW91 functional and 6-311++G(2d,2p) basis set using Gaussian 09 [13].

Acknowledgements

We thank the Generalitat de Catalunya for financial support through the CERCA Programme and recognition (2014 SGR 893) and MINECO (CTQ2016-75499-R (AEI/FEDER-UE)) for financial support and support through Severo Ochoa Excellence Accreditation 2014–2018 (SEV-2013-0319). This work was supported by JST PRESTO (JPMJPR16S3), Japan.

Keywords: IR spectroscopy • XAS• XRD • MOF

References

[1] a) A. Urakawa, *Curr. Opin. Chem. Eng*., **2016**, *12*, 31-36; b) U. Bentrup, *Chem. Soc. Rev.*, **2010**, *39*, 4718-4730; c) C. Garino, E. Borfecchia, R. Gobetto, J. A. van Bokhovend, C. Lambertia, *Coord. Chem. Rev.*, **2014**, *277*, 130-186. d) F. C. Meunier, *Chem. Soc. Rev.*, **2010**, *39*, 4602-4614. e) J. -D. Grunwaldt, M. Caravati, S. Hannemann, A. Baiker, *Phys. Chem. Chem. Phys.*, **2004**, *6*, 3037-3047.
[2] a) M. A. Bañares, *Catal. Today*, **2005**, *100*, 71-77; b) B. M. Weckhuysen, *Phys. Chem. Chem. Phys.*, **2003**, *5*, 4351-4360; c) K. F. Kalz, R. Kraehnert, M. Dvoyashkin, R. Dittmeyer, R. Gläser, U. Krewer, K. Reuter, J. D. Grunwaldt, *Chem. Cat. Chem*., **2017**, *9*, 17-29; d) S. Bordiga, E. Groppo, G. Agostini, J. A. van Bokhoven, C. Lamberti, *Chem. Rev.* **2013**, *113*, 1736-1850; e) A. Schneemann, V. Bon, I. Schwedler, I. Senkovska, S. Kaskel, R. A. Fischer, *Chem. Soc. Rev.*, **2014**, *43*, 6062-6096. f) J. A. van Bokhoven, C. Lamberti, *X-Ray Absorption and X-Ray Emission Spectroscopy: Theory and Applications*, Vol. 1, Chapter 12, John Wiley & Sons, Chichester (UK), **2016**, p. 303.
[3] W. van Beek, O. V. Safonova, G. Wiker, H. Emerich, *Phase Transitions*, **2011**, *84*, 726-732.
[4] a) S. Bordiga, C. Lamberti, F. Bonino, A. Travert, F. Thibault-Starzyk, *Chem. Soc. Rev.*, **2015**, *44*, 7262-7341. b) A. Vimont, F. Thibault-Starzyk, M. Daturi, *Chem. Soc. Rev.*, **2010**, *39*, 4928-4950. c) C. Lamberti, A. Zecchina, E. Groppo, S. Bordiga, *Chem. Soc. Rev.*, **2010**, *39*, 4951–5001.
[5] a) M. A. Newton, W. van Beek, *Chem. Soc. Re*v., **2010**, *39*, 4845-4863; b) M. A. Newton, *Top. Catal.*, **2009**, *52*, 1410-1424; c) M. A. Newton, A. J. Dent, S. G. Fiddy, B. Jyoti, J. Evans, *Phys. Chem. Chem. Phys.*, **2007**, *9*, 246-249; d) M. A. Newton, A. J. Dent, S .G. Fiddy, B. Jyoti, J. Evans, *Catal. Today*, **2007**, *126*, 64-72; e) M. A. Newton, A. J. Dent, S. G. Fiddy, B. Jyoti, J. J. Evans, *Mater. Sci.* **2007**, *42*, 3288-3298; f) M. A. Newton, C. Belver-Coldeira, A. Martínez-Arias, M. Fernández-García, *Nat. Mater.*, **2007**, *6*, 528-532.
[6] S. Hannemann, M. Casapu, J. -D. Grunwaldt, P. Haider, P. Trüssel, A. Baiker, E. Welter, *J. Synchrotron. Rad.*, **2007**, *14*, 345-354.
[7] H. Furukawa, F. Gándara, Y. Zhang, J. Jiang, W. L. Queen, M. R. Hudson, O. M. Yaghi, *J. Am. Chem. Soc.* , **2014**, *136*, 4369-4381.

[8] a) J. H. Cavka, S. Jakobsen, U. Olsbye, N. Guillou, C. Lamberti, S. Bordiga, K. P. Lillerud, *J. Am. Chem. Soc*. **2008**, *130*, 13850-13851; b) L. Valenzano, B. Civalleri, S. Chavan, S. Bordiga, M. H. Nilsen, S. Jakobsen, K. P. Lillerud, C. Lamberti, *Chem. Mater*. **2011**, *23*, 1700-1718; c) S. Bordiga, F. Bonino, K. P. Lillerud, C. Lamberti, *Chem. Soc. Rev*. **2010**, *39*, 4885; d) P. Ji, J. B. Solomon, Z. Lin, A. Johnson, R. F. Jordan, W. Lin, *J. Am. Chem. Soc.* **2017**, *139*, 11325-11328; e) A. M. Plonka, Q. Wang, W. O. Gordon, A. Balboa, D. Troya, W. Guo, C. H. Sharp, S. D. Senanayake, J. R. Morris, C. L. Hill, A. I. Frenkel, *J. Am. Chem. Soc.* **2017**, *139*, 599-602; f) C. Hennig, S. Weiss, W. Kraus, J. Kretzschmar, A. C. Scheinost, *Inorg. Chem.* **2017**, *56*, 2473-2480; g) for solution EXAFS measurements of the discreet SBU-type Zr_6-oxocarboxylates, see: C. Hennig, S. Weiss, W. Kraus, J. Kretzschmar, A. C. Scheinost, *Inorg. Chem*. **2017**, *56*, 2473.

[9] A. J. Graham, J. C. Tan, D. R. Allanc, S. A. Moggach, *Chem. Commun.*, **2012**, *48*, 1535-1537.

[10] F. Giordanino, E. Borfecchia, K. Lomachenko, A. Lazzarini, G. Agostini, E. Gallo, A. Soldatov, P. Beato, S. Bordiga, C. Lamberti, *J. Phys. Chem. Lett.*, **2014**, *5*, 1552-1559.

[11] a) S. Marx, W. Kleist, A Baiker, *J. Catal.*, **2011**, *281*, 76-87. b) C. Prestipino, L. Regli, J. G. Vitillo, F. Bonino, A. Damin, C. Lamberti, A. Zecchina, P. L. Solari, K. O. Kongshaug, S. Bordiga, *Chem. Mater.*, **2006**, *18*, 1337-1346. c) E. Borfecchia, S. Maurelli, D. Gianolio, E. Groppo, M. Chiesa, F. Bonino, C. Lamberti, *J. Phys. Chem. C*, **2012**, *116*, 19839-19850.

[12] O. V. Gutov, S. Molina, E. C. Escudero-Adán, A. Shafir, *Chem. Eur. J.* **2016**, *22*, 1-7.

[13] Gaussian 09 (Revision A.02), M. J. Frisch, G. W. Trucks, H. B. Schlegel, G. E. Scuseria, M. A. Robb, J. R. Cheeseman, G. Scalmani, V. Barone, B. Mennucci, G. A. Petersson, H. Nakatsuji, M. Caricato, X. Li, H. P. Hratchian, A. F. Izmaylov, J. Bloino, G. Zheng, J. L. Sonnenberg, M. Hada, M. Ehara, K. Toyota, R. Fukuda, J. Hasegawa, M. Ishida, T. Nakajima, Y. Honda, O. Kitao, H. Nakai, T. Vreven, J. Montgomery, J. A., J. E. Peralta, F. Ogliaro, M. Bearpark, J. J. Heyd, E. Brothers, K. N. Kudin, V. N. Staroverov, R. Kobayashi, J. Normand, K. Raghavachari, A. Rendell, J. C. Burant, S. S. Iyengar, J. Tomasi, M. Cossi, N. Rega, N. J. Millam, M. Klene, J. E. Knox, J. B. Cross, V. Bakken, C. Adamo, J. Jaramillo, R. Gomperts, R. E. Stratmann, O. Yazyev, A. J. Austin, R. Cammi, C. Pomelli, J. W. Ochterski, R. L. Martin, K. Morokuma, V. G. Zakrzewski, G. A. Voth, P. Salvador, J. J. Dannenberg, S. Dapprich, A. D. Daniels, Ö. Farkas, J. B. Foresman, J. V. Ortiz, J. Cioslowski, D. J. Fox, Gaussian, Inc., Wallingford CT, **2009**.